Diffusionless Rotator-Crystal Transitions in Colloidal Truncated Cubes

- 3 Abhishek K. Sharma^{1,2} and Fernando A. Escobedo^{1,*}
- ⁴ R.F. Smith School of Chemical and Biomolecular Engineering, Cornell University, Ithaca, NY 14853, USA
- ² Current affiliation: Department of Chemical Engineering, Albert Nerken School of Engineering, The Cooper
- 6 Union for the Advancement of Science and Art, New York NY 10003, USA

* Corresponding author: fe13@cornell.edu

Abstract

Upon osmotic compression, rotationally symmetric faceted colloidal particles can form translationally-ordered, orientationally-disordered rotator mesophases. This study explores the mechanism of rotator-to-crystal phase transitions where orientational order is gained in a translationally ordered phase, using rotator-phase forming truncated cubes as testbed. Monte Carlo simulations were conducted for two selected truncations (s), one for s = 0.527 where the rotator and crystal lattices are dissimilar and for s = 0.572 where the two phases have identical lattices. These differences set the stage for a qualitative difference in their rotator-crystal transitions, highlighting the effect of lattice distortion on phase transition kinetics. Our simulations reveal that significant lattice deviatoric effects could hinder the rotator-to-crystal transition and favor arrangements of lower packing fraction instead. Indeed, upon compression it is found that for s = 0.527 the rotator phase does not spontaneously transition into the stable, densely packed crystal due to the high lattice strains involved, but instead transitions into a metastable solid phase to be colloquially referred to as "orientational salt" for short, which has a similar lattice as the rotator phase and

- 1 exhibits two distinct particle orientations having substitutional order, alternating regularly throughout the
- 2 system. This study paves the way for further analysis of diffusionless transformations in nanoparticle

Recent developments in nanoparticle synthesis have fueled recent efforts for the realization of particle

3 systems, and how lattice-distortion could influence crystallization kinetics.

1. Introduction

4

5

6

7

8

9

10

11

12

13

14

15

16

17

18

19

20

21

22

geometries with unprecedented intricacy, precision, and reproducibility.¹⁻⁶ Production of faceted, polyhedral particles has especially opened up new opportunities for the creation of complex (super) lattices at the nanoscale owing their shape-driven preferential packing at high concentrations (controlled by appropriate osmotic pressure conditions). These self-assembled nanostructures find useful applications in plasmonics, 5,7 photonics, 8,9 and serve as model systems for the study of emergent phenomena as they exhibit thermodynamic and kinetic behaviors analogous to those of atomic systems, including the formation of ordered structures resulting from local particle properties like size and valence, 10,11 with classically understood mechanisms such as nucleation and growth. When suspended as colloids, polyhedral particles exhibit a rich mesophase behavior as a function of their geometric properties. 12,13 While all particle geometries are fully disordered at low packing fractions, with increasing osmotic pressure, the systems could structure into a variety of ordered phases that minimize their free-energy, e.g., by maximizing their configurational entropy.¹⁴ The particles that have known densest-packed lattices often transition to such crystalline structures at high pressures, attaining both orientational and translational order. 12 Depending of particle geometry, at moderate osmotic pressures the system can form mesophases. ¹² If particles have a high degree of asphericity (e.g., high or low aspect ratios), one could expect formation of liquid crystalline phases such as nematic and smectic phases. These phases possess varying degrees of orientational order with no or limited translational order compared to the

1 crystal. Upon further compression these liquid crystalline phases may transition to fully ordered crystals.

¹⁵⁻¹⁹Recent computational studies have revealed that the degree of anisotropy of such structures can have

implications for not only their phase behavior but also their kinetics. 15,20,21

2

3

4

5

6

7

8

9

10

11

12

13

14

15

16

17

18

19

20

21

22

23

24

Similarly, upon compression, rotationally symmetric particles can attain translational order before achieving full orientational order, forming rotator or plastic phases, where particles occupy well defined lattice positions but do not orient in the same direction. ^{22,23} Upon further osmotic compression, the rotator phases will often transition to crystal phases, where particles can pack more efficiently albeit losing rotational entropy. This rotator lattice, however, may not be identical to that of the crystal phase. Besides differences in lattice constants due to increased system's density, the underlying lattices for rotator and crystalline phases may not be affine contractions-expansions of each other. Thus, even as the primary change is in the system at the rotator-crystal transition is orientational order of the system, the differences in translational order could be significant and influence the kinetics of such transitions. As particles do not migrate great distances (compared to lattice spacing) in transitioning from rotator to crystal phase and vice versa, these phase transitions can be designated as diffusionless. Further, as these transitions are accompanied by a discontinuous change in specific volume (which is the partial derivative of free energy with respect to pressure), they are also first-order phase transitions. We henceforth freely borrow the classification from the literature on diffusionless/displacive transformations in metals and alloys. ^{24,25} A phase transformation is called *lattice-distortive* if the shape of the unit cell is distorted in the process. In contrast, if particles rearrange within the unit cell, then it is termed as a shuffle transformation. The latticedistortive transformations can further be composed of dilational and deviatoric components, where the former refers to the expansion or contraction of the lattice, and the latter refers to transformations where the lattice may have an undistorted line (such as a rotation or shear). Dilation itself could be homogeneous (isotropic) or heterogeneous (anisotropic). These classifications are not clear-cut, as there can be transformations that may not fit clearly in one category.

In this paper, we study such diffusionless rotator-crystal transitions in hard faceted nanoparticles; specifically, for particle shapes in the truncated cubes family, which exhibit a rich phase behavior as a function of the degree of truncation s. 12,13,26,27 Previous studies have focused on the isotropic to rotator transition that takes place via nucleation and growth. 22,28 In this paper we complement those studies by investigating the rotator-to-crystal phase transitions. These transitions have been studied in the past for other shapes, 23 revealing the interesting influence of similarity/dissimilarity between local directional entropic forces and crystal lattice on the nature of the transition.

$$s = 0.527 \text{ (TC52)}$$
 $s = 0.572 \text{ (TC57)}$

Figure 1: Shapes from the truncated cubes family studied in this paper, s = 0.527 (TC52, left) and s = 0.572 (TC57, right).

We focus on two specific truncations: s = 0.527 and s = 0.572 to be henceforth referred to as TC52 and TC57, respectively, whose phase behavior and coexistence conditions are well established (see Figure 1). These shapes are selected because, first, their preferred orientations in the rotator phase are of the same symmetry. Second and more importantly, despite being quite proximal in truncation space (s), the lattice geometry for rotator and crystal phases is nearly identical for TC57 but is different for TC52. This difference allows us to study the influence of lattice distortion on the rotator-to-crystal phase transition mechanism.

- 1 The rest of this manuscript is organized as follows: Section 2 describes the simulation methods and order
- 2 parameters employed in this study. Section 3 reports the observations and Section 4 discusses the results
- 3 and provides an outlook for future work.

4 2. Methods

5 **2.1 Model**

6 Any two particles *i* and *j* in our systems interact through a hard pair-potential energy given by:

8

- 9 The overlap is detected by using the separating axis theorem.²⁹ The particle shape for a given value of
- truncation parameter s of a cube was obtained through formulae described in an earlier study. 26 Note that
- the two shapes under study (TC52 with s=0.527 () and TC57 with s=0.572) lie in between the cases of
- the cuboctahedra (s = 0.5) and the truncated octahedra (s = 0.667), with TC52 being near the shape with
- the lowest densest packing and TC57 being near the shape with the lowest asphericity. ^{26,27}

2.2 Monte Carlo Simulations

- 15 Metropolis³⁰ Monte Carlo (MC) simulations were performed in the isothermal-isobaric (NpT) ensemble,
- where N is the total number of particles, p is the pressure, and T is the temperature. All lengths are scaled
- by $a_{1/2}$, half of the side length of the original cube from which the particles are truncated. Thus, the
- dimensionless pressure is given by $p=\beta p_a a_{1/2}^3$, where p_a is the unscaled pressure and $\beta=\frac{1}{k_BT'}$ where
- k_B is Boltzmann's constant. The supersaturation is defined as

 $\Delta\mu_{od} = \mu_o - \mu_d,\tag{2}$

1

2

3

4

5

6

7

8

9

10

11

12

13

14

15

16

17

18

19

20

21

22

23

24

where μ_o and μ_d are chemical potentials associated with most and least ordered phases in the transition, respectively. The chemical potentials and free energies are all scaled by k_BT . In the context of rotatorcrystal transition, the crystal is considered the most ordered phase. The volume fractions for the coexisting phases of interest were obtained from an earlier thermodynamic integration study³¹ and the corresponding chemical potentials provided by the authors of those publications. The simulations used periodic boundary conditions to mimic bulk behavior. Unless specified otherwise, each MC cycle included N translation, N rotation (along box coordinate axes), and 2 volume moves. Isotropic and anisotropic (triclinic) volume moves were used for isotropic and translationally ordered phases respectively. To accelerate the exploration of different particle orientations in the rotator phase, we additionally perform N 60°-rotations along the particle's body diagonal which facilitate rotation between orientations with similar facet presentations, such that four out of six square facets are approximately replaced by the hexagonal facets and would roughly align with their neighbors. This rotation was motivated by the presence of three distinct orientations in the rotator phases as described in Section 3.2.2. Please note that the very same symmetry space can be explored by other rotations, particularly a 90° rotation along the edge diagonal as discussed later. The crystal phase is initiated with configurations close to the best packing of the crystal phase previously reported. ²⁶ The configuration is then equilibrated at p = 9.0 and gradually expanded until it orientationally melts into the rotator phase. For TC52, such a melting nearly always results in grain boundaries. To prevent the formation of grain boundaries, we pick the lowest pressure where the crystal phase was observed and gradually expand it without any translational moves. The triclinic volume moves allow for proper distortion of the lattice to yield a rotator phase with a defect-free lattice. This lattice is equilibrated with the standard NpT ensemble simulations and compressed gradually until p = 9.0 but (for TC52) they end up transitioning to the orientational salt at much lower pressures as discussed in the Results section.

2.3 Order Parameters and Correlations

- We use Steinhardt-style³² order parameters to capture the particle orientational order.²⁸ We employ i_4 as
- 3 it can effectively capture O_h (octahedral) symmetry for all particles in the truncated cubes family. For
- 4 a given particle j, i_4 is defined as:

5
$$i_{4,m}(j) = \frac{\sum_{n=1}^{3} Y_{4,m}(\theta_n, \phi_n)}{\sqrt{\sum_{m=-4}^{4} |\sum_{n=1}^{3} Y_{4,m}(\theta_n, \phi_n)|^2}}$$
 (3)

- 6 where $Y_{4,m}(heta_n,\phi_n)$ are spherical harmonics with symmetry index 4, and $heta_n$ and ϕ_n are polar and
- 7 azimuthal angles of the 3 particles axis *n* with respect to the reference coordinate frame.
- 8 The orientation correlation between two particles k and l is defined as:

9
$$d_i(k,l) = \sum_{m=-4}^4 i_{4,m}(k) \cdot i_{4,m}^*(l)$$
 (4)

- where the asterisk (*) denotes the complex conjugate in both cases.
- 11 These parameters are evaluated for each particle in the system. For the calculation of the contiguous grain,
- 12 a particle is considered contiguous (and aligned) to another if $d_i > 0.6$ and they are within the cutoff
- distance $r_c = 8$ for the first neighbors. More details on these order parameters are provided in the previous
- 14 studies. 28,33
- 15 For capturing the rotator-salt transition, we develop an order parameter to capture the planarity of aligned
- first neighbors. As will be depicted later (in Figure 11), each salt particle in the ideal case has exactly 4
- aligned neighbors occupying the same plane. We determine the orientational alignment using the cut off
- for $d_i > 0.6$. A particle with 4 or 3 aligned neighbors would be a candidate for being salt-like, and we select
- 19 the case of 3 neighbor particles to allow for some flexibility. We determine the co-planarity of the aligned
- 20 neighborhood by calculating the volume of the tetrahedron comprising the central particle and its aligned
- 21 neighbors. For 3 neighboring particles this yields one number, and for 4 neighbors we take the average of

- 1 two sets of four particles (always inclusive of the central particle). If this average volume is less than
- $0.38a_{1/2}^3$ then the aligned neighborhood is deemed to be planar and thus the central particle to be salt-
- 3 like. Neighboring salt-like particles are considered to be "contiguous" for the calculation of fraction of
- 4 particles in the largest contiguous grain, x_q .

2.4 Umbrella Sampling

- 6 We performed umbrella sampling²⁸ for the TC57 rotator-crystal transition and TC52 rotator-salt transition
- 7 using the fraction of particles in the largest contiguous grain (x_g) as order parameter.
- We conducted the calculations for a system of 2304 TC57 particles at three pressures, $p \in \{4.5, 4.6, 4.66\}$,
- 9 noting that the rotator-crystal phase coexistence pressure is ≈ 4.5 . Starting with the rotator phase, where
- all orientations are in equal proportion, we divided the transition path along x_g with equally spaced,
- overlapping windows of ~0.04 width. The overlap between windows is half its range, i.e., each window
- shares the first half with the previous window. We advance the simulation to the next window when the
- 13 system has explored the overlap region for at least 2000 MC cycles. In any window, we restrict the allowed
- value of x_g with an effective infinite square well potential the width of the window. Unbiased isothermal-
- isobaric simulations were performed at each window to collect histograms of the relative frequency of x_q
- 16 (binned and resolved to a particle level, i.e., to 1/2304). We sampled x_q every 2 MC cycles and ran each
- window for 2 million MC cycles. The resulting probability distribution $P_i(x_q)$ in each i^{th} window is then used
- to obtain the relative free energy [$\sim -\ln (P_i(x_q))$] within the bounds of the window, and composite free
- 19 energy curve is obtained by matching values in the middle of the overlapping regions of neighboring
- 20 windows. Similar procedure was followed for TC52 rotator-salt transformation, with 1000 particles at p =
- 21 4.1.

2.5 Visualization of Configurations

1

- 2 Simulated configurations are visualized using Visual Molecular Dynamics (VMD) software.³⁷ To distinguish
- 3 between orientational disorder and order, particles were colored based on their alignment with the box
- 4 axis. For any particle, the dot product of its three axes unit vectors is taken with respect to the box x-axis.
- 5 This dot product has a theoretical minimum of $\frac{1}{\sqrt{3}}$ and a maximum of unity. A colormap is then used to color
- 6 the particles red if the dot product equals $\frac{1}{\sqrt{3}}$ and blue if it equals one, with shades of yellow and green in
- 7 between. In essence, this coloring depicts the level of 'orthogonality' of any particle with respect to the box
- 8 coordinate system. Note that the configuration snapshots shown were sometimes reorientated for clarity,
- 9 so the apparent coloring of particles in the figures may not be comparable across panels or figures.
- 10 To particularly highlight the differences between rotator, "salt" (to be defined later), and crystalline phases,
- and the internal distribution of orientations in the rotator and salt states, we also employed a different
- 12 coloring scheme that provides a sharp color contrast between the three orientations favored by the rotator
- 13 phase in each lattice.

14 3. Results and Discussion

3.1 Equations of State and Phase Behavior

16 **3.1.1 TC52**

- 17 Equations of state regimes for TC52 (N = 1000) are shown in Figure 2. While we observe the previously
- reported²⁶ isotropic, rotator, and crystal phases, (Figure 3(a,b,d)) upon compression the rotator phase
- 19 spontaneously transitions at pressures above $p \approx 4.0$ into a novel *orientational* salt composed of two
- 20 distinct orientations (Figure 3(c)). (See supplementary movies for TC52 rotator-salt transition video). Like

the cesium chloride (CsCl) crystal, TC52 particles are arranged in the body-centered tetragonal (BCT) lattice with one orientation occupying the body center and the other occupying the corners of the unit cell. We suspect that this configuration might have been missed in previous studies due to the absence of our additional rotation moves that allow for a more thorough sampling of phase space. In rotator phases of truncated cubes, it has been reported that while particles are not all orientationally aligned, they do prefer to roughly occupy certain orientational sectors. These sectors may be rather distinct with scarce overlaps, implying that it would be unlikely for particles in a simulation with small rotational moves to go from one orientational sector to another. We therefore included additional rotation moves to sample across different orientational sectors in the rotator phase as detailed in Section 2.2. We note that the salt formation is not observed if insufficient rotation moves are conducted in the simulations, where the rotator transitions to the crystal phase. The equation-of-state branch for the salt was corroborated by expanding this phase until melting, which revealed that it transforms back to a rotator phase at $p \approx 3.9$, indicating a small amount of hysteresis. Since the coexistence pressure between the rotator and crystal phases is $p_{co,rc} \approx 2.9$ (and between the isotropic and rotator phases is $p_{co,ir} \approx 1.1$) and the salt phase only appears above $p \approx 4.1$, then the latter must be regarded as a metastable state. Indeed, it is instructive to estimate the contributions to the athermal free energies of the crystal and salt phases: G = pV - TS. At, say p = 4.4 where $\phi_{\text{crys}} = 0.743$ and $\phi_{\text{salt}} = 0.713$, the pV values indicate favorability (a smaller G) for the crystal as it is smaller than that for the salt. Conversely, the S term indicates favorability for salt as it has larger orientational entropy (having two distinct orientational states) than the crystal phase (having a unique orientational state). However, disregarding differences in entropic contributions from vibrational and orientational fluctuations, the difference in pV (at p = 4.2) is estimated to be about twice as larger as that coming from the orientational degrees of freedom $\left[\frac{p(v_{salt}-v_{crys})}{k_BT}\sim 1.5\right] > \frac{S_{salt}-S_{crys}}{k_B} \sim \ln(2)$, where v_{salt} and v_{crys} are the per particle

1

2

3

4

5

6

7

8

9

10

11

12

13

14

15

16

17

18

19

20

21

22

volumes of the salt and crystal phases, and $s_{cryst} \sim 0$ and s_{salt} are estimated from the number of distinguishable orientational macrostates per particle in the crystal (1) and salt (2), respectively. This result indicates a net thermodynamic favorability for the crystal state. Importantly, unlike the cases when a metastable phase is a mesophase that can act as a catalyst for the crystal phase formation,²¹ in this case, the metastable salt acts rather as a poison for the stable crystal.

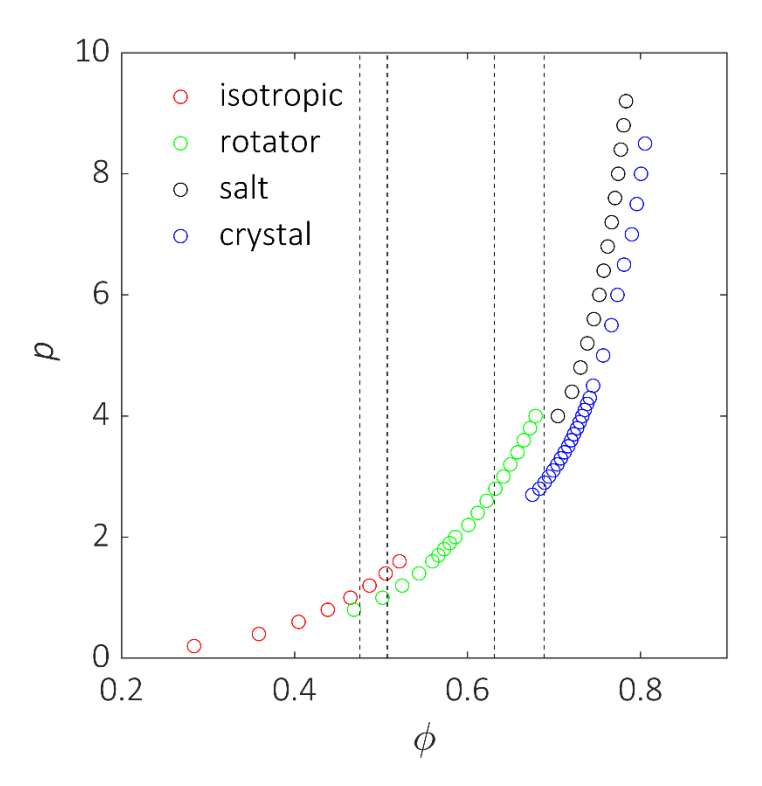


Figure 2: Equation of state for TC52 obtained from compression and expansion simulation runs as described the text. The vertical dashed lines mark the packing fractions at the coexisting isotropic-rotator and rotator-crystal phase transitions. In the salt branch, the data at pressures p > 4 is from the configuration formed by a rotator transitioning to salt at p=4.4. The data point for p=4 is obtained upon expansion of the salt thus formed.

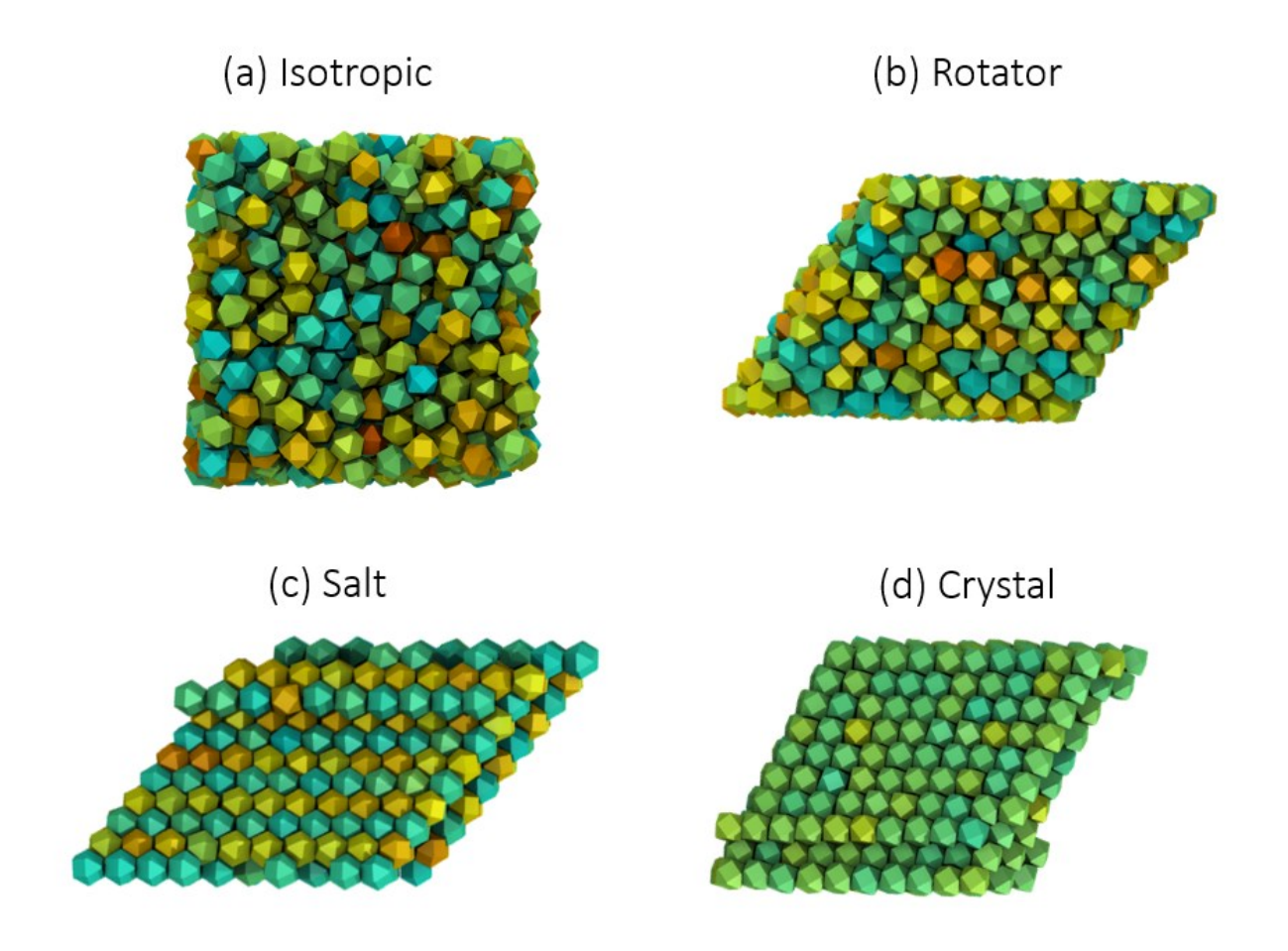


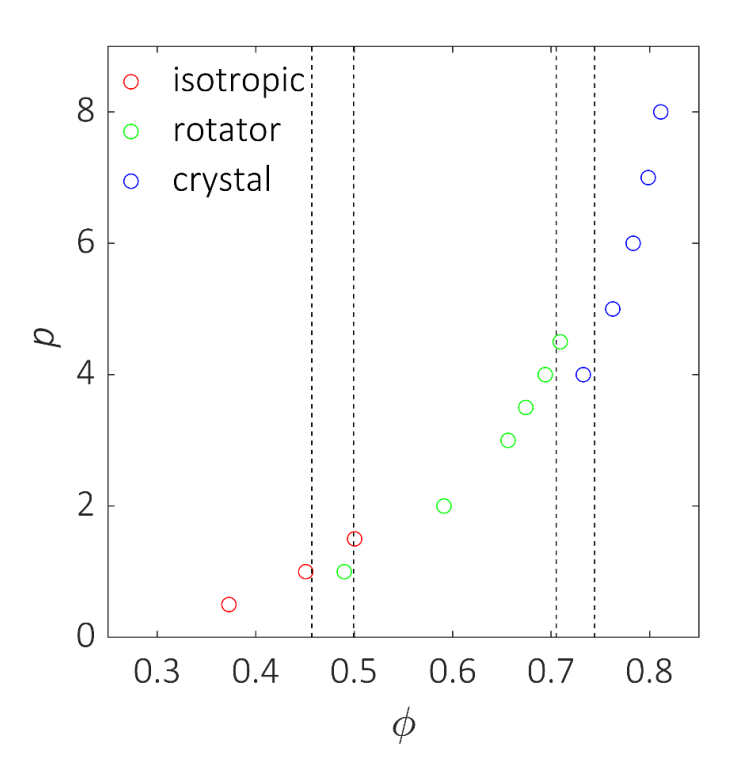
Figure 3: Sample configurations for various phases obtained for TC52. (a) Isotropic phase at p=1.0, $\phi=0.465$; (b) Rotator phase at p=4.5, $\phi=0.465$; (c) Orientational Salt at p=4.8, $\phi=0.731$; (d) Crystal phase at p=4.5, $\phi=0.745$. Particle coloring correlates with their alignment with respect to the box coordinate as described in Section 2.5.

3.1.2 TC57

Equations of state for TC57 (N=2304) are shown in Figure 4. In this case, we only observe the branches for the known isotropic, rotator, and crystal phases (Figure 5). The coexistence pressures between isotropic and rotator phases $p_{co,ir} \approx 1.1$ and between rotator and crystal phases is $p_{co,rc} \approx 4.5$. For the rotator-to-crystal transition, one observes in the rotator phase the presence of small, localized domains of particles having the same orientation, occurring as transient fluctuations; upon increasing the pressure, these

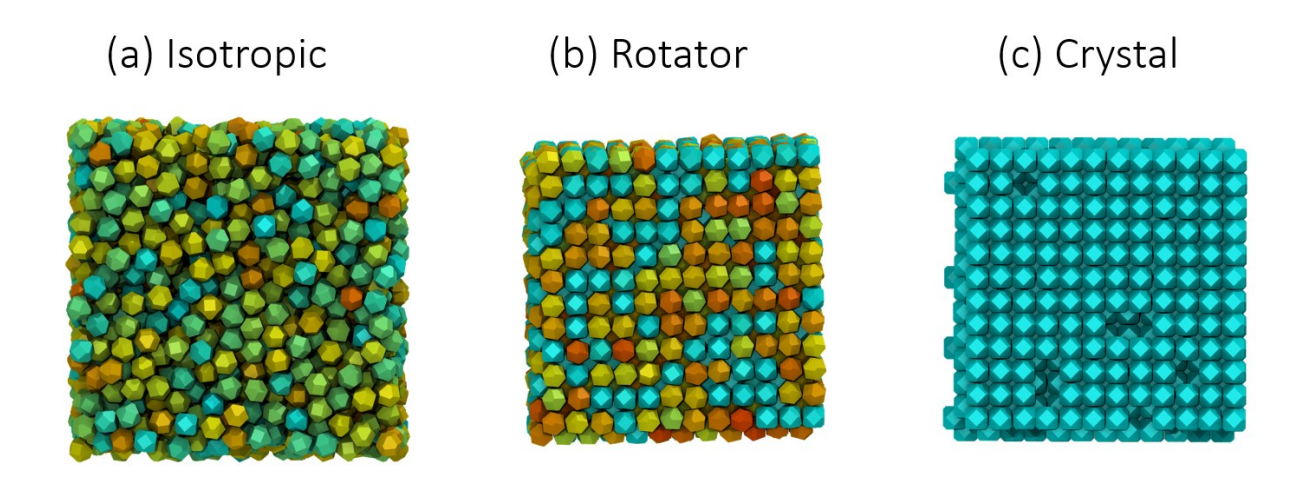
- domains tend to coarsen (as described later in Section 3.3.2) and become longer-lived. Eventually, the system transitions to a single, simulation-box spanning domain with a specific orientation characteristic of
- 3 the crystalline state . (See supplementary movies for TC57 rotator-crystal transition video).
- Unlike the TC52 case, in this system no salt-phase formed spontaneously. We conjecture that while such a salt phase could potentially exist, it may be as a rather inaccessible, short-lived metastable fluctuation. As discussed in the next sections, for TC52 one reason why the salt phase, rather than the crystal phase, is favored upon compression of the rotator phase is because of the dissimilarity in lattice parameters between the rotator and crystal phases. ForTC57 the lattice parameters of rotator and crystal phase as rather similar,

leaving little 'configurational space' in between to accommodate a distinct, deep metastable basin.



9

Figure 4: Equation of state for TC57 obtained from compression and expansion simulation runs as described in the text. The vertical
dashed lines mark the packing fractions at the coexisting isotropic-rotator and rotator-crystal phase transitions.



- Figure 5: Sample configurations for various phases observed for TC57: (a) Isotropic phase at p=1.0, $\phi=0.451$; (b) Rotator phase at
- 3 p=4.5, $\phi=0.709$; (c) Crystal phase at p=5.0, $\phi=0.763$. Particle coloring correlates with their alignment with respect to the box
- 4 coordinate axes as described in Section 2.4.

3.2 Analysis of Phases

7 3.2.1 Crystal and Rotator Lattices

- 8 The rotator phases for both shapes are reported to be positioned on a body-centered tetragonal (BCT)
- 9 lattice. The crystal phase for TC52 is a distorted BCT lattice whereas the TC57 lattice remains BCT.²⁶
- 10 We can illustrate the difference between these lattices by analyzing their coordination shells. Figure 6(a)
- shows the coordination number as a function of distance for TC52 for the rotator and crystal phases at p =
- 12 3.4.

1

5

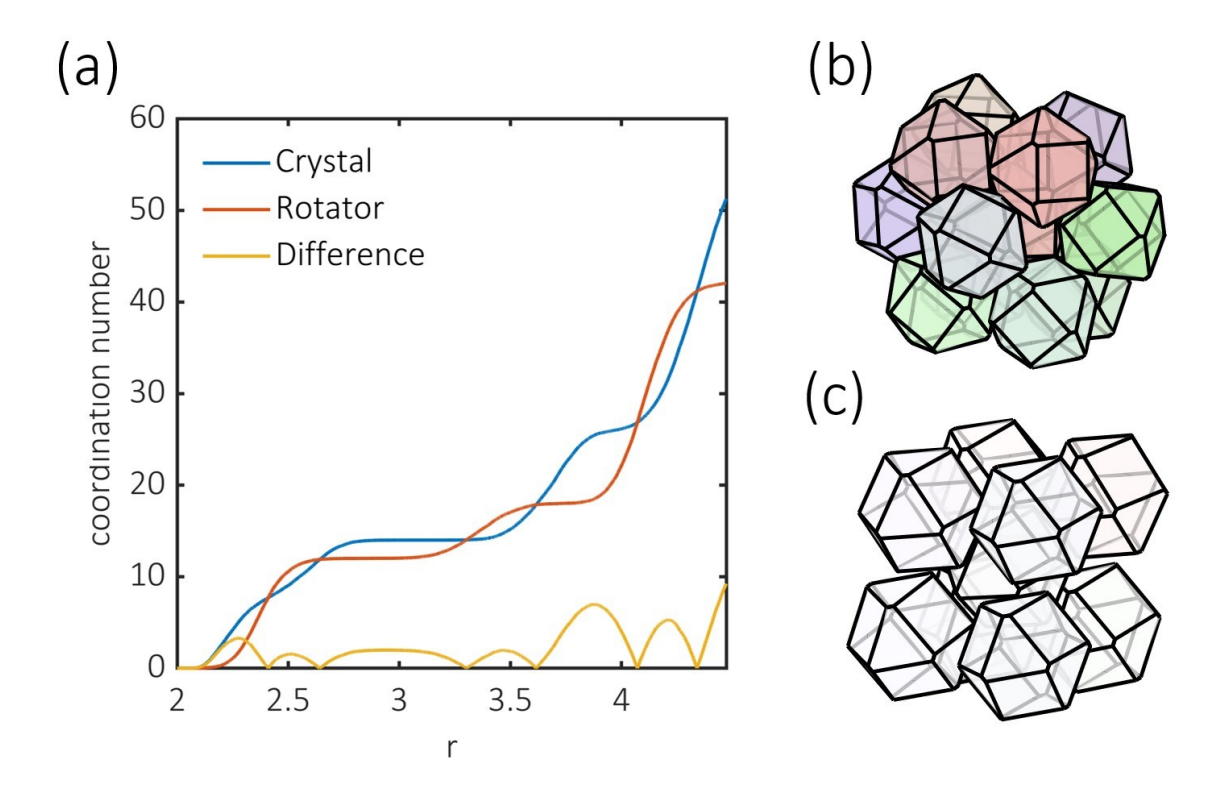


Figure 6: Structure of the coordination shell for TC52 rotator (ϕ = 0.658) and crystal (ϕ = 0.712) phases at p=3.4: (a) Coordination number as a function of interparticle distance. Illustration of nearest neighbors for the rotator phase (b) and the crystal phase (c), with particle coloring as described in Section 2.5.

For TC52 we find that there is a qualitative difference between the two phases in that the rotator phase has 12 nearest neighbors situated at roughly the same distance whereas the crystal phase has 8 nearest neighbors. The arrangement of the nearest neighbors for the rotator and crystal phase is shown in Figure 6(b) and Figure 6 (c) respectively. The rotator phase's nearest neighbors are quite similar in their arrangement to a face-centered cubic lattice, which is not unexpected given that FCC and BCT structures are related.³⁸ The crystal phase has the neighbors arranged as if the original particle is placed at the body center and the rest are arranged at the corners, albeit not on a cubic cell (hence distorted).

In contrast, for TC57 we find that the coordination shell for both rotator and crystal phases is identical (Figure 7), with both having the nearest coordination shell with 12 neighbors arranged on a BCT lattice.

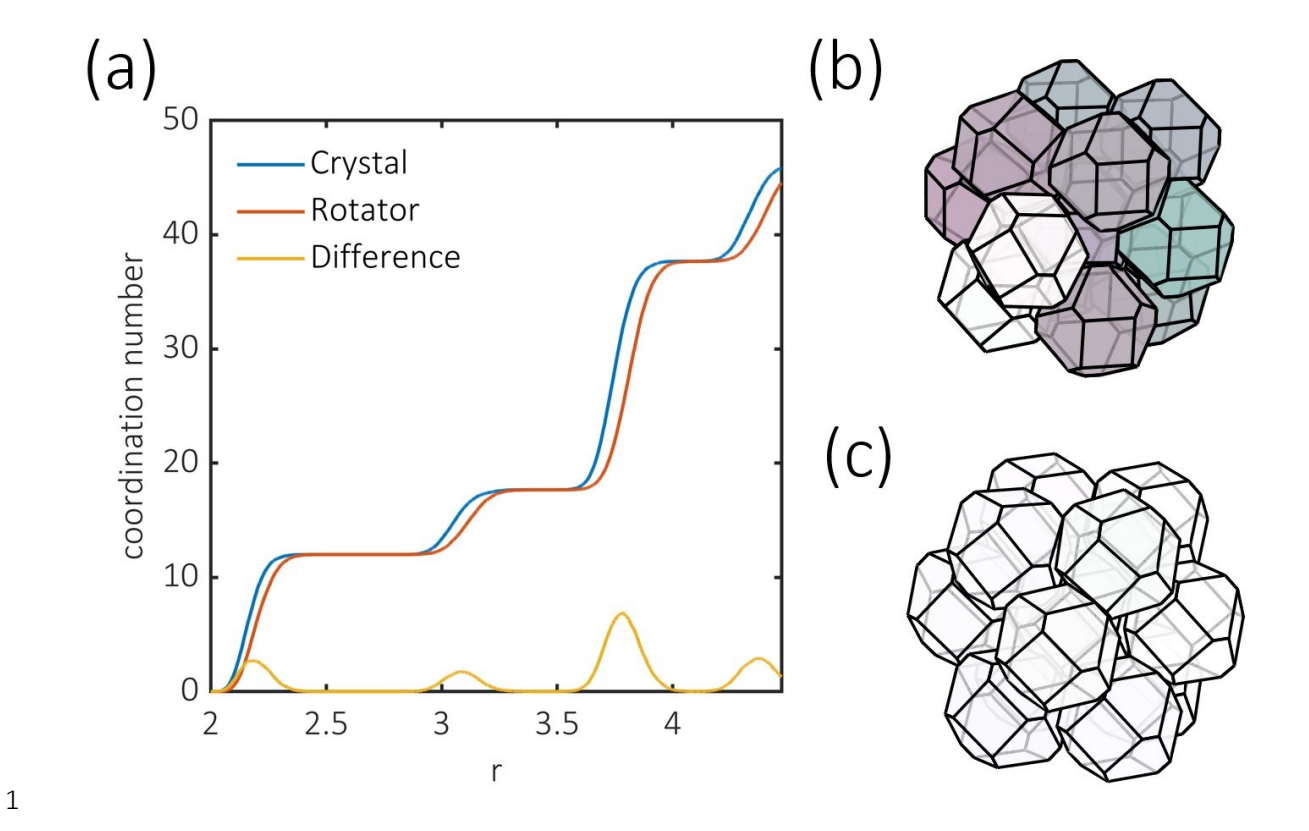


Figure 7: Structure of the coordination shell for TC57 rotator (φ = 0.72) and crystal (φ = 0.763) phases at p=5.0: (a) Coordination
number as a function of interparticle distance. Illustration of nearest neighbors for the rotator phase (b) and for the crystal phase
(c), with particle coloring as described in Section 2.5.

3.2.2 Rotator Phase Orientational Sectors

- The arrangement of orientation vectors populated by the rotator phases for both shapes is shown in Fig. 8, illustrating the similarity in their orientational distributions. The particles prefer 18 orientational sectors which can be understood as arising from three distinct orientations and their \mathcal{O}_h symmetry, leading to three sets of six orthogonal sectors.
- The identification of the three distinct orientations allows for a visually contrasting coloring of the rotator phases that reveals the distribution of the three orientations as shown in Figure 9. The three orientations for both shapes are always percolating (with respect to the nearest neighbor connections) in the lattice with >90% of particles present in the percolating network at a given time. The three orientations are related

to each other by a 90° rotation along the edge diagonal (Figure 9(c)), equivalently, a 60° rotation along the body diagonal (as used in the simulation methods for rotational moves). Note that these orientations do not particularly align with the bond vectors of the nearest neighbors. Furthermore, the lattices that particles with different orientations occupy have a slight deviation with respect to each other, which is clearly revealed for larger systems (Figure 10). This indicates that there is a packing inefficiency, or excess volume present whenever the neighboring particle orientations are different.

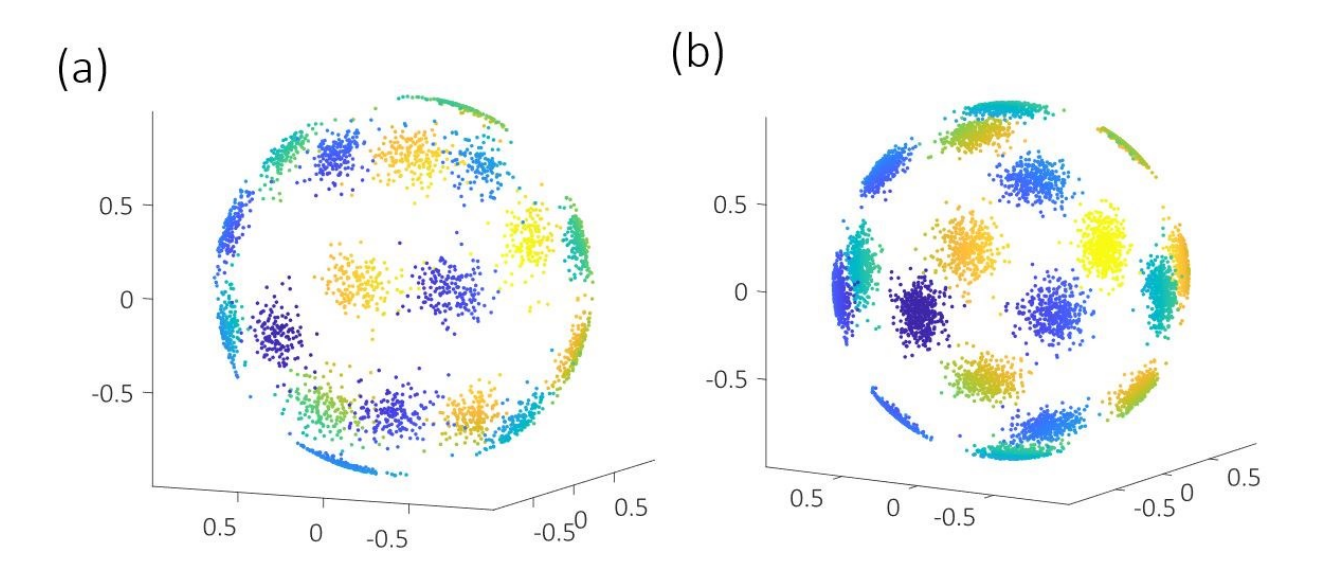
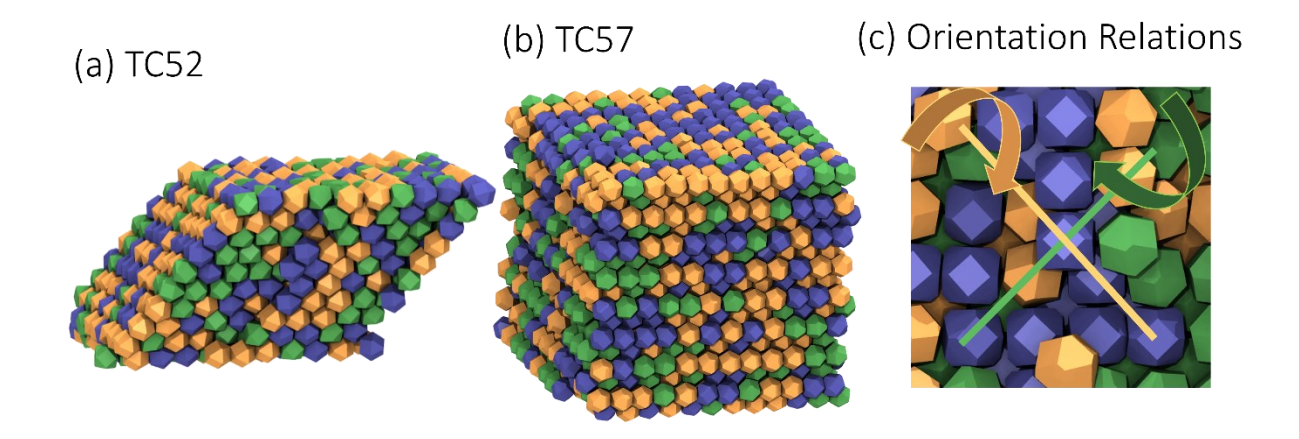


Figure 8: Preferred orientational sectors for rotator phases: (a) TC52 at p=4.0, $\phi=0.679$, N=1000 (b) TC57 at p=4.5, $\phi=0.709$, N=2304. Points are colored as a function of their orientation with respect the box axis on the bottom right, with blue in the foreground (negative values) and yellow in the background (positive values).



2 Figure 9: Rotator phases colored distinctly with respect to the three preferred particle orientations (yellow, green and blue). (a)

 $3\qquad \textit{TC52; (b) TC57; (c) rotational relations between the 3 particle orientations, showing how they are related via a <math>90\,^{\circ}$ rotation along}

4 the edge diagonal.

1

5

6

7

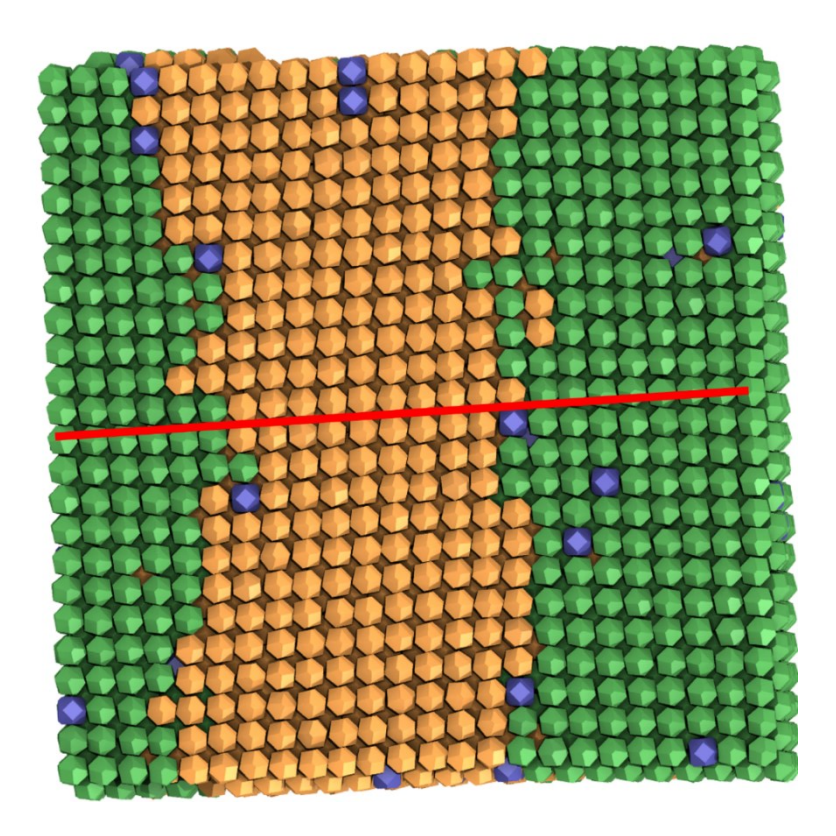


Figure 10: Grain boundary formed by the junction of two crystal orientations emerging from a simulation of rotator to crystal transition for N=18432 TC57 particles at p=5.0, ϕ = 0.763. The red line aligns with the line of particles in the yellow lattice, which clearly deviates from the green lattice. Particle coloring is described in Section 2.4.

3.2.3 Orientational Salt for TC52

1

2

3

4

5

6

7

8

9

10

11

12

13

14

15

16

17

18

19

Compression of the TC52 rotator phase beyond p = 4.0 results in the spontaneous formation of a crystalline state that we denote as the orientational salt given that the two distinct orientations are arranged in a substitutionally ordered lattice. The analysis of coordination shells and sample arrangement of nearest neighbors is shown in Figure 11. We notice that the salt has the same number of nearest neighbors as the rotator phase, and the variation of coordination number as a function of distance is also qualitatively similar to that of the rotator phase, except for a small 'bump' near r=3.1. The visualization of the nearest neighbors reveals an interesting arrangement of the two orientations. From the standpoint of the BCT lattice, one could describe the orientational salt as one orientation occupying the corners and the other orientation occupying the body centers. This 1:1 salt is reminiscent of cesium chloride (albeit being BCT instead of BCC). This arrangement has the orientational distribution shown in Figure 12 with 12 preferred orientations, instead of 18 observed for the rotator, and thus two distinct orientations under the O_h symmetry. Note that the similar spread of directions around these two orientations in Fig. 12(a) indicates that they exhibit comparable orientation fluctuations. The salt has a lower packing fraction when compared to crystal at comparable pressures. The spontaneous formation of this metastable salt from the rotator phase, instead of the stable crystal, likely stems from kinetic effects, with a transformation to the salt structure requiring a minimal lattice distortion while a transformation to the crystal structure requiring a significant lattice distortion and overcoming a larger concomitant free-energy barrier.

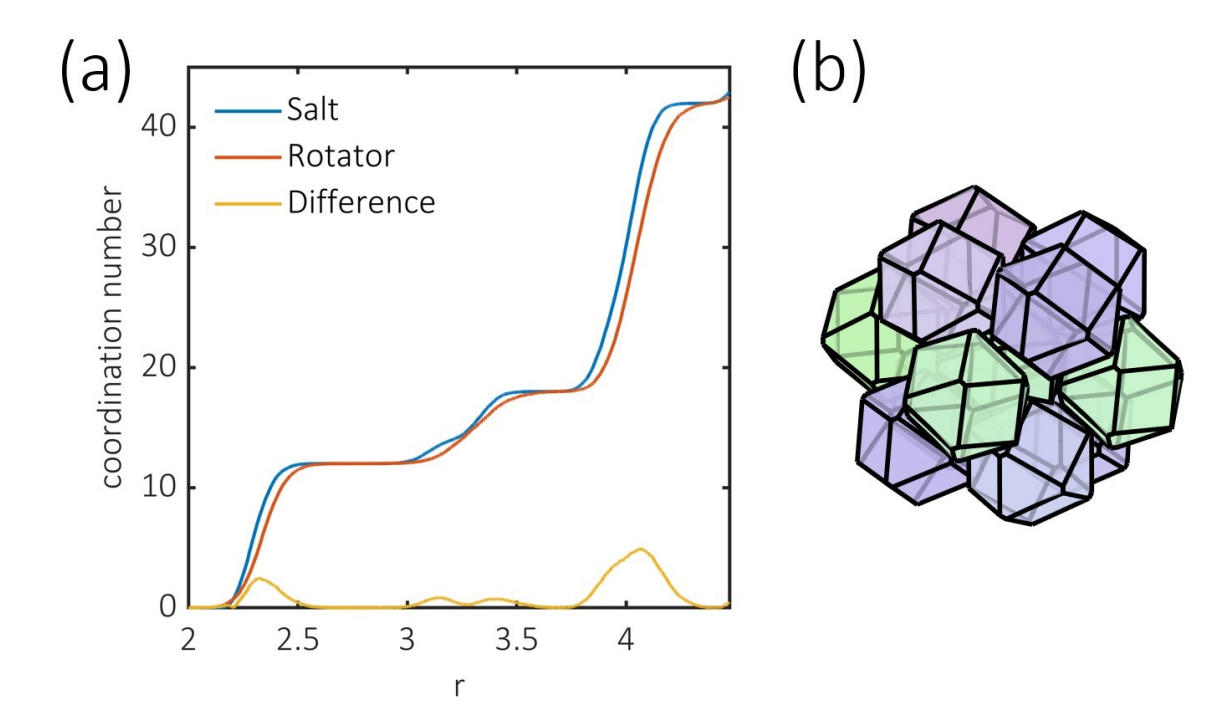


Figure 11: Structure of the coordination shell for TC52 orientational salt at p=4.8, $\phi=0.731$: (a) Coordination number as a function of interparticle distance. (b) Depiction of nearest neighbors with particle coloring as described in Section 2.4.

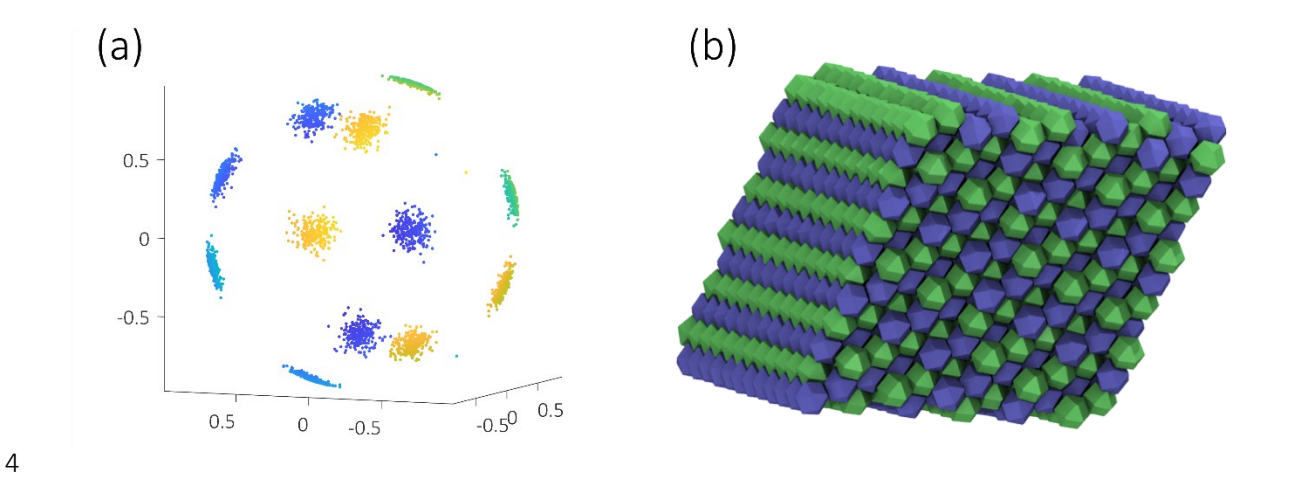


Figure 12: (a) Particle orientations for the TC52 orientational salt at p=4.8, $\phi=0.731$. Points are colored based on their orientation with respect to the box x-axis, with blue in the foreground and yellow in the background. (b) Representative salt configuration with particles colored according to their orientations associated with the two sectors present.

7

8

9

10

3.3 Diffusionless Transformations

- 3 The rotator-crystal transitions are inherently lattice-dilational (or contractional), given the change in
- 4 volume fraction and distances between the nearest neighbors. For TC52 in particular, there is a significant
- 5 difference in the lattice structure of the rotator and crystal, and one may expect a significant deviatoric
- 6 component to the transformation.

3.3.1 Lattice displacements are smaller for rotator-to-salt than for rotator-to-crystal

transition in TC52

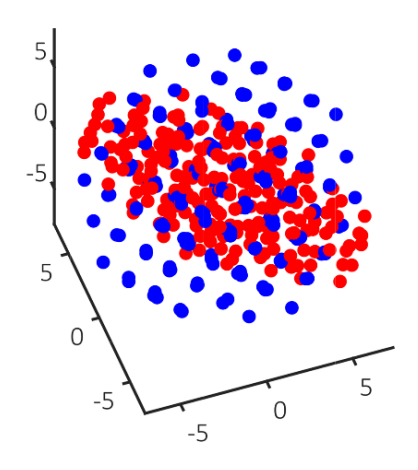
transformations. To do this, we take two configurations and pick a particle as the origin (i.e., we shift and

The visualization of lattice displacements between two configurations could be useful in characterizing the

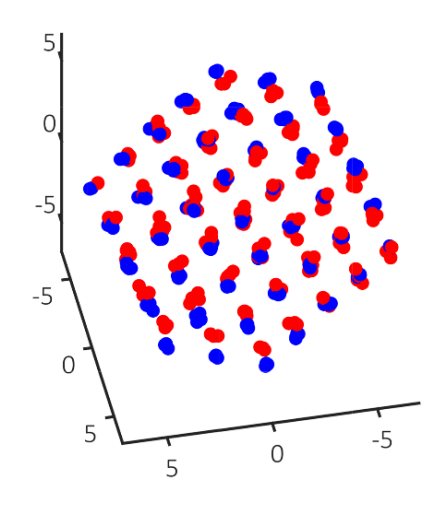
- rewrap the configurations according to periodic boundary conditions such that a particular particle is at the
- origin). We then calculate the displacements of all particles needed to go from one state to another,
- rewrapping them as needed, and construct scatter plots with the initial and final particle positions to trace
- 14 the spatial transformation. We choose to color the rotator phase positions in blue color and the salt/crystal
- 15 phases in red. Note that the displacements are relative to one reference particle and tend to increase for
- distant particles as the effects add up. For clarity we only show the nearest 200 particles (to the reference
- particle) in each scatter plot and amplified the displacements by a factor of two. Thus, the initial set of
- 18 rotator positions in blue starts off as roughly spherical cluster, and the eventual shape distortion of the
- 19 cluster of red points reflects the nature and magnitude of the lattice transformation. Displacement plots
- for all particles with unamplified displacements are given in the Supplementary Information.
- 21 Lattice displacements for a TC52 rotator-crystal transition are plotted in Figure 13 (a), obtained from
- melting of the crystal and recompression of the rotator phase to p = 3.4. The scatter plot has been

rotated to clearly show the elongation/contraction of the lattice. This pattern is similar to a uniaxial contraction flow, as evidenced by the ellipsoidal shape of the particle cluster in the final crystal which compresses drastically along one axis while expanding in the orthogonal directions. In contrast, the transformation from the rotator to the orientational salt does not lead to a significant lattice displacement (Figure 13(b)); interestingly, the displacements could be described here as being part of a rotation (see SI). On average, the particle displacements required for the rotator-crystal transition are about five times larger in magnitude than those for the rotator-salt transition. This disparity in lattice distortion is likely the reason why the salt configuration is kinetically more accessible in our simulations which mimic pseudo diffusive particle dynamics. Finally, lattice displacements for TC57 from rotator to crystal are shown in Figure 13(c). The average displacement is comparable to that of the TC52 rotator-salt transition, where the displacements largely seem to be isotropically compressing the lattice. For all displacements, we can also visualize them through interpolating videos in the Supplementary materials.

(a) TC52: Rotator-Crystal



(b) TC52: Rotator-Salt



(c) TC57: Rotator-Crystal

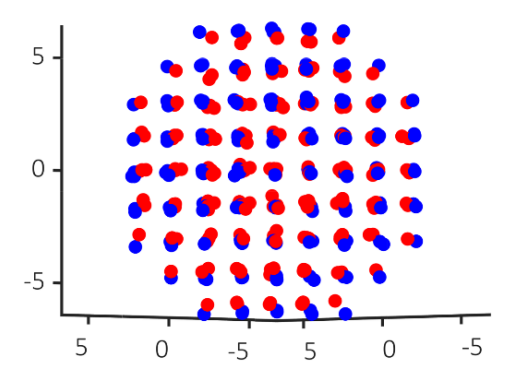


Figure 13: Lattice displacements for the diffusionless transformations starting from the rotator phase.). The rotator lattice particle positions are shown with blue points and the final lattice (crystal/rotator) particle position are shown in red points. Each plot is centered on a specific particle with the axes in scaled units of the simulation as described in Section 2.2. The particle displacements are amplified by a factor of 2 to make lattice transformations clearer. (a) Rotator-to-crystal transformation in TC52 at p=3.4 (ϕ from 0.658 to 0.712. (b) Rotator-to-salt transformation in TC52 at p=4.4 (ϕ from 0.69 to 0.713), and (c) Rotator-to-crystal transformation in TC57 at p=5.0 (ϕ from 0.72 to 0.763).

7

8

9

10

11

12

13

14

15

16

17

18

19

20

21

22

23

24

1

2

3

4

5

6

3.3.2 Transition Free Energy Calculations and Correlations

We attempted unsuccessfully to complete a number of calculations to map the nucleation free energy barrier for the different phase transitions of interest, using as order parameter the largest nucleus of the incipient phase in the system as described in previous studies.³⁶ Some of the difficulties were related to issues previously encountered in the disorder to order transition of colloidal cubes. 33,35 In particular, the simulations invariably led to the emergence of multiple nuclei within the same simulation box. As such, no reliable information on the characteristics of a presumptive critical nucleus could be ascertained from the simulations. In particular, for the TC52 system we are unable to show that the kinetic free-energy for rotator-to-salt phase transition is lower than that for the rotator-to-crystal transition (as one would expect from the transitions observed in compression simulations). Thus, we only report results on the successful calculation of barriers using the contiguous grain size x_q as the bulk order parameter (as defined in Sections 2.3-2.4). Note that a free-energy barrier calculation based on a bulk-phase order parameter like x_a characteristically different from those of nucleation calculations (where a single critical nucleus forms) in that the barrier heights are now size dependent. In a previous study³³ it was demonstrated that this dependence is systematic, and in the range of 10^3 particles and above, the barrier heights are 'extensive'; i.e., scale with system size. Despite this limitation, this calculation is still valuable in characterizing key

- 1 features of transitions with a bulk character such as the structure of the transition state, the onset of nuclei
- 2 percolation and the formation and resolution of grain boundaries. The barriers calculated can also be used
- 3 to identify trends in degree of local order (clustering), spatial correlations between ordered domains, and
- 4 the onset of percolating order if the system approaches spinodal fluctuations. 34,35
- 5 The free energy profiles for the TC57 rotator-crystal transformation at various pressures are shown in
- Figure 14(a). We find that the rotator phase is still stable at p=4.5, while it becomes metastable at p=4.5
- 7 4.6 with a barrier of ~15 k_BT , which reduces further to less than 5 k_BT at p=4.66. Calculations beyond
- 8 this pressure are difficult to perform as the system becomes unstable, indicating that the system
- 9 approaches a spinodal instability and undergoes a spontaneous transition. 15,20,34,35,39

11

12

13

14

15

16

17

18

19

20

21

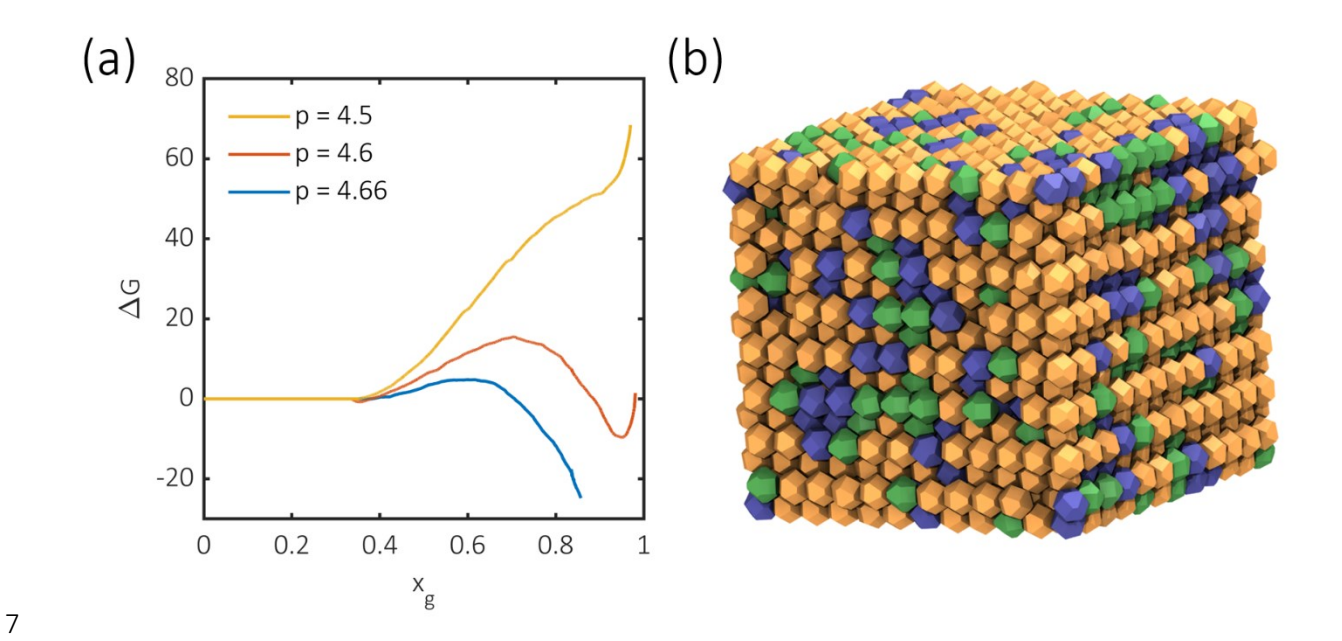
22

23

As Figure 14(b) illustrates for the rotator-crystal transition for TC57, one can observe that at the top of the free energy barrier the dominant crystalline grain percolates the entire system. The absence of a compact, well-defined nucleus, however, should not be seen as a *bug* but rather a *feature* of this transition. This is because crystallization of the rotator state simply entails the coupling of orientational fluctuations of neighboring particles, a (free-energy) inexpensive process that happens throughout the system, with small nuclei being able to reorient to merge with neighboring ones and thus couple their orientations over long distances. We conjecture that the interfacial free-energy between rotator and crystal phases of TC57 is rather small, not unlike that between the isotropic and solid phases of hard cubes, ³⁷ a system which also exhibit delocalized crystallization. For the rotator-salt transformation for TC52, a similar behavior is observed with a percolating grain occurring atop the free energy barrier (Figure 15(a)), albeit at a much lower x_g and hence exhibiting a weaker percolation (Figure 15(b)). Interestingly, even before the TC52 rotator approaches the barrier top, the system forms a substitutionally disordered solution of the two dominant orientations (Figure 15(c)), which gradually become substitutionally ordered (alternating positions) as the salt grains grow.

The orientational correlations of the rotator phase in Fig. 16 also reveal a gradual increase in the correlation lengths as the system approaches the transition pressures, another hallmark of a spinodal instability. This increase is largely absent for rotator phase of TC52 (at the rotator-salt transition pressure), revealing that the local motions of the particles would not be conducive to long-range alignment and rather hinder crystallization.





 $\textbf{8} \qquad \textbf{\textit{Figure 14}: (a) Free energy profiles (in k_BT units) for the rotator-crystal phase transition for TC57 using the largest contiguous grain}$

 x_g as the order parameter at various pressures. (b) A representative configuration atop of the barrier at p=4.6 near $x_g \approx 0.66$

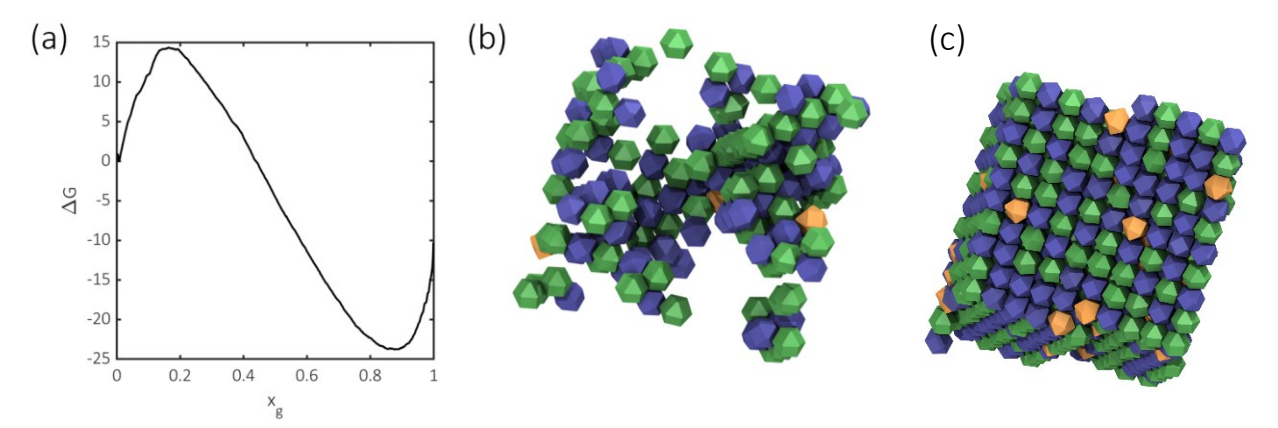


Figure 15: (a) Free energy profile (in k_BT units) for the rotator-salt transition for TC52 using the largest contiguous grain x_g as the order parameter at p=4.1, Representative configurations of the largest contiguous salt grain (b) and of the entire system (c) atop of the barrier $x_g \approx 0.17$.

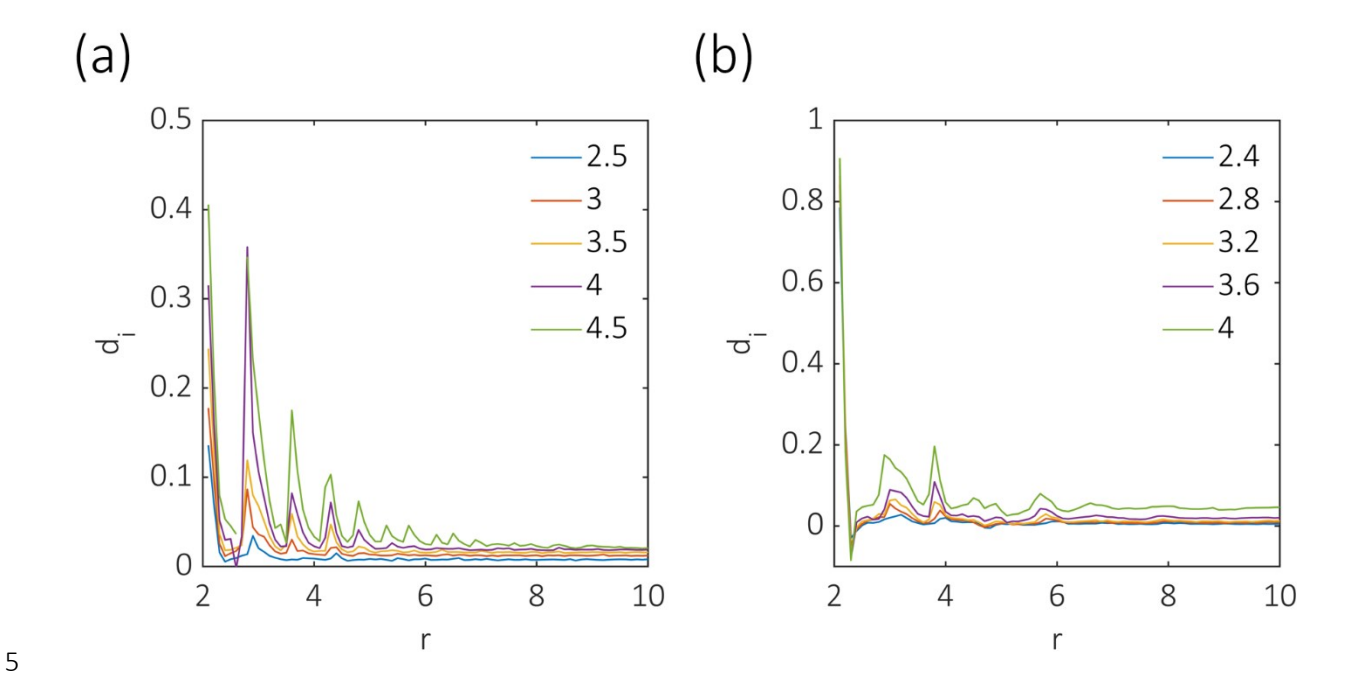


Figure 16: The orientational correlation d_i as a function of distance at various pressures (given as legend and with lines of different colors) for (a) TC57 up to the rotator-crystal coexistence pressure (~4.5) and (b) TC52 up to the rotator-salt coexistence pressure (~4.0).

4. Conclusions and Future Work

1

2

3

4

5

6

7

8

9

10

11

12

13

14

15

16

17

18

19

20

21

22

23

In this paper, we have investigated the rotator-crystal transition for two representative truncations of cubes (TC52 and TC57). We found the existence of a novel orientational salt that forms spontaneously upon compression of the TC52 rotator phase; importantly, this spontaneity suggests that such a phase is likely to be observable experimentally (i.e., kinetically accessible). We analyzed these rotator, salt, and crystal phases in terms of their coordination shells to reveal interesting differences and similarities among their underlying lattice structures. Particularly, for TC52 we find that the coordination shell structure for the rotator is much closer to that of the orientational salt than that of the crystal, which could be the reason why the rotator phase prefers transitioning to the orientational salt in compression simulations. In comparison, the relative similarity of the rotator and crystal phase coordination shells for TC57 facilitates a spontaneous rotator-crystal transition. We analyzed the transitions in the context of established classification schemes of lattice-distortive transformations, finding a significant deviatoric distortion of rotator-crystal transition in TC52 compared to a significantly lower lattice distortion needed for salt formation. Finally, we performed free energy barrier calculations for the rotator-crystal transition of TC57 and rotator-salt transition in TC52 and reported on the evolution of orientational correlations of the rotator phases, to characterize the approach to spinodal instability. Future studies of the TC52 and related systems could focus on performing calculations of the free energy landscape along the salt- and crystalline-distinguishing order parameters and determine the evolution of this landscape as a function of pressure. Such plots would also unequivocally reveal the role of kinetics and the nature of the pathways that favor the formation of the metastable salt configuration. It would also be useful to determine the interfacial free energy between particle domains having different orientations. These systems would provide a unique model system with three equipotential states, behaving as a 3-state Potts model embedded in a body centered tetragonal lattice. Further exploration of critical phenomena

- 1 related to these transitions could also be of interest as their analysis would be facilitated by the Potts model
- 2 framework where such phenomena are prevalent.

4

5

6

7

8

9

10

11

12

13

14

15

16

17

18

19

20

21

22

This study also provides a steppingstone toward a comprehensive characterization of phase transformations involving rotator phases. While the presence of distinct preferred particle orientations in such phases has been previously reported, the spatial and statistical distribution of such orientations could be seen as fingerprints that foretell key features of their phase transitions. There is also a motivation to rationalize the previously reported rotator phase orientations for other systems in the context of their underlying lattices, and if there exist systems where the preferential orientations are distributed unequally. Furthermore, spatial segregation of such orientations could be studied to quantify the interfacial free energy for particles neighboring such "grain boundaries". One the one hand, the existence of a novel orientational salt configuration provides a motivation for the search of similar sub-optimally packed structures that are kinetically trapped at high concentrations. On the other hand, it would also be of interest to identify particle designs for which orientational salts are thermodynamically stable phases. Such a search could be started from a metastable salt phase and its free-energy mapped via integrations over changes of different interparticle potential parameters, looking to find conditions that minimize the salt-phase free energy, possibly treating different orientations as distinct pseudo-components. 40,41 Such studies could also systematically reveal the extent to which salt-phases are present as metastable basins, while allowing for variations in lattice parameters and particle orientations. The structure of salt-like phases could be nontrivial as they need not be the densest packed nor follow common geometrical patterns like most crystalline phases of hard polyhedra. 13 Finally, the experimental realization of these phases also poses a non-trivial design challenge. To that end, it will be useful to model the emergence of these phases with the additional involvement of enthalpic effects⁴² as these are ubiquitous in experimental systems.⁴³

5. Supplementary Materials

- 2 The supplementary materials include simulation and interpolation movies for the transitions, and additional
- 3 plots for lattice displacement fields:
- TC52 Rotator-Salt.avi: Spontaneous transition of the rotator phase of TC52 to salt at p = 4.1
- TC57_Rotator-Crystal.avi: Spontaneous transition of the rotator phase of TC57 to crystal at p = 5.0
- TC52_Rotator-Salt_Interpolation.avi: Interpolation between the positions and orientations of the rotator phase of TC52 and the salt it transitions to at p = 4.1.
- TC57_Rotator-Crystal_Interpolation.avi: Interpolation between the positions and orientations of the rotator phase of TC57 and the crystal it transitions to at p = 5.0
 - Supplementary_Information.pdf: Unscaled lattice displacements for diffusionless transformations and spatial transformation analysis.

12 6. Acknowledgements

- 13 Funding support from NSF Awards No. CBET-1907369 and CHE-2101829 is gratefully acknowledged. This
- research was also supported in part by grant NSF PHY-1748958 to the Kavli Institute for Theoretical Physics
- 15 (KITP). We are thankful to Dr. Anjan Gantapara and Prof. Marjolein Dijkstra for sharing the coexistence data
- 16 for various truncations of cubes.

10

7. References

- ¹ A. Tao, P. Sinsermsuksakul, and P. Yang, "Polyhedral silver nanocrystals with distinct scattering
- 3 signatures," Angewandte Chemie International Edition 45(28), 4597–4601 (2006).
- ⁴ J. Henzie, M. Grünwald, A. Widmer-Cooper, P.L. Geissler, and P. Yang, "Self-assembly of uniform
- 5 polyhedral silver nanocrystals into densest packings and exotic superlattices," Nat Mater 11(2), 131–137
- 6 (2012).

- 7 ³ Y. Sun, and Y. Xia, "Shape-controlled synthesis of gold and silver nanoparticles," Science (1979) **298**(5601),
- 8 2176–2179 (2002).
- 9 ⁴ J. Henzie, M. Grünwald, A. Widmer-Cooper, P.L. Geissler, and P. Yang, "Self-assembly of uniform
- polyhedral silver nanocrystals into densest packings and exotic superlattices," Nat Mater 11(2), 131–137
- 11 (2012).
- 12 ⁵ B. Pietrobon, M. McEachran, and V. Kitaev, "Synthesis of size-controlled faceted pentagonal silver
- nanorods with tunable plasmonic properties and self-assembly of these nanorods," ACS Nano 3(1), 21–26
- 14 (2009).
- 15 ⁶ D. Seo, C.P. Ji, and H. Song, "Polyhedral gold nanocrystals with Oh symmetry: From octahedra to cubes,"
- 16 J Am Chem Soc **128**(46), 14863–14870 (2006).
- ⁷ K. Bian, H. Schunk, D. Ye, A. Hwang, T.S. Luk, R. Li, Z. Wang, and H. Fan, "Formation of self-assembled gold
- nanoparticle supercrystals with facet-dependent surface plasmonic coupling," Nat Commun **9**(1), (2018).
- 19 ⁸ R.K. Cersonsky, J. Dshemuchadse, J. Antonaglia, G. Van Anders, and S.C. Glotzer, "Pressure-tunable
- photonic band gaps in an entropic colloidal crystal," Phys Rev Mater **2**(12), 125201 (2018).

- ⁹ T.J. Kempa, S.K. Kim, R.W. Day, H.G. Park, D.G. Nocera, and C.M. Lieber, "Facet-selective growth on
- 2 nanowires yields multi-component nanostructures and photonic devices," J Am Chem Soc 135(49), 18354–
- 3 18357 (2013).
- 4 ¹⁰ V.N. Manoharan, "Colloidal matter: Packing, geometry, and entropy.," Science **349**(6251), 1253751
- 5 (2015).
- 6 ¹¹ Z. Zeravcic, V.N. Manoharan, and M.P. Brenner, "Colloquium: Toward living matter with colloidal
- 7 particles," Rev Mod Phys **89**(3), 1–14 (2017).
- 8 ¹² U. Agarwal, and F.A. Escobedo, "Mesophase behaviour of polyhedral particles," Nat Mater **10**(3), 230–
- 9 235 (2011).
- 10 13 P.F. Damasceno, M. Engel, and S.C. Glotzer, "Predictive self-assembly of polyhedra into complex
- structures," Science (1979) **337**(6093), 453–457 (2012).
- 12 L. Onsager, "the Effects of Shape on the Interaction of Colloidal Particles," Ann N Y Acad Sci **51**(4), 627–
- 13 659 (1949).
- 14 ¹⁵ A. Cuetos, and M. Dijkstra, "Kinetic Pathways for the Isotropic-Nematic Phase Transition in a System of
- 15 Colloidal Hard Rods: A Simulation Study," Phys Rev Lett **98**(9), 095701 (2007).
- 16 I.A.C. Veerman, and D. Frenkel, "Phase diagram of a system of hard spherocylinders by computer
- 17 simulation," Phys Rev A (Coll Park) **41**, 15 (1990).
- 18 ¹⁷ B.S. John, and F.A. Escobedo, "Phase behavior of colloidal hard tetragonal parallelepipeds (cuboids): A
- 19 Monte Carlo simulation study," Journal of Physical Chemistry B **109**(48), 23008–23015 (2005).
- 20 ¹⁸ B.S. John, A. Stroock, and F.A. Escobedo, "Cubatic liquid-crystalline behavior in a system of hard cuboids,"
- 21 Journal of Chemical Physics **120**(19), 9383–9389 (2004).

- 1 ¹⁹ B.S. John, C. Juhlin, and F.A. Escobedo, "Phase behavior of colloidal hard perfect tetragonal
- parallelepipeds," Journal of Chemical Physics **128**(4), 044909 (2008).
- 3 ²⁰ A. Cuetos, E. Sanz, and M. Dijkstra, "Can the isotropic-smectic transition of colloidal hard rods occur via
- 4 nucleation and growth?," Faraday Discuss **144**(0), 253–269 (2009).
- 5 21 A.K. Sharma, and F.A. Escobedo, "Effect of particle anisotropy on the thermodynamics and kinetics of
- ordering transitions in hard faceted particles.," J Chem Phys **158**(4), 044502 (2023).
- 7 ²² V. Thapar, and F.A. Escobedo, "Localized orientational order chaperones the nucleation of rotator phases
- 8 in hard polyhedral particles," Phys Rev Lett **112**(4), 048301 (2014).
- 9 ²³ A.S. Karas, J. Dshemuchadse, G. Van Anders, and S.C. Glotzer, "Phase behavior and design rules for plastic
- 10 colloidal crystals of hard polyhedra: Via consideration of directional entropic forces," Soft Matter 15(27),
- 11 5380-5389 (2019).
- 12 ²⁴ L. Delaey, "Diffusionless Transformations," in *Phase Transformations in Materials*, (Wiley-VCH Verlag
- 13 GmbH & Co. KGaA, Weinheim, FRG, 2005), pp. 583–654.
- 14 ²⁵ J.W. Christian, G.B. Olson, and M. Cohen, "Classification of Displacive Transformations: What is a
- 15 Martensitic Transformation ?," Le Journal de Physique IV **05**(C8), C8-3-C8-10 (1995).
- 16 ²⁶ A.P. Gantapara, J. De Graaf, R. Van Roij, and M. Dijkstra, "Phase behavior of a family of truncated hard
- cubes," Journal of Chemical Physics **142**(5), 054904 (2015).
- 18 ²⁷ A.P. Gantapara, J. De Graaf, R. Van Roij, and M. Dijkstra, "Phase diagram and structural diversity of a
- 19 family of truncated cubes: Degenerate close-packed structures and vacancy-rich states," Phys Rev Lett
- 20 **111**(1), 1–5 (2013).

- 1 ²⁸ A.K. Sharma, V. Thapar, and F.A. Escobedo, "Solid-phase nucleation free-energy barriers in truncated
- 2 cubes: Interplay of localized orientational order and facet alignment," Soft Matter 14(11), 1996–2005
- 3 (2018).
- 4 ²⁹ S. Gottschalk, M.C. Lin, and D. Manocha, "OBB tree: A hierarchical structure for rapid interference
- 5 detection," Proceedings of the 23rd Annual Conference on Computer Graphics and Interactive Techniques,
- 6 SIGGRAPH 1996 (8920219), 171–180 (1996).
- 7 ³⁰ N. Metropolis, A.W. Rosenbluth, M.N. Rosenbluth, A.H. Teller, and E. Teller, "Equation of state
- 8 calculations by fast computing machines," J Chem Phys **21**(6), 1087–1092 (1953).
- 9 ³¹ F. Smallenburg, L. Filion, M. Marechal, and M. Dijkstra, "Vacancy-stabilized crystalline order in hard
- 10 cubes," Proc Natl Acad Sci U S A **109**(44), 17886–17890 (2012).
- 11 ³² P.J. Steinhardt, D.R. Nelson, and M. Ronchetti, "Bond-orientational order in liquids and glasses," Phys Rev
- 12 B **28**(2), 784–805 (1983).
- 13 ³³ A.K. Sharma, and F.A. Escobedo, "Disorder Foreshadows Order in Colloidal Cubes," Journal of Physical
- 14 Chemistry B **122**(39), 9264–9273 (2018).
- 15 ³⁴ R. Ni, S. Belli, R. Van Roij, and M. Dijkstra, "Glassy dynamics, spinodal fluctuations, and the kinetic limit of
- nucleation in suspensions of colloidal hard rods," Phys Rev Lett **105**(8), 7–10 (2010).
- 17 ³⁵ A.K. Sharma, and F.A. Escobedo, "Low Interfacial Free Energy Describes the Bulk Ordering Transition in
- 18 Colloidal Cubes," J Phys Chem B **125**(19), 5160–5170 (2021).
- 19 ³⁶ S. Auer, and D. Frenkel, "Numerical prediction of absolute crystallization rates in hard-sphere colloids.,"
- 20 J Chem Phys **120**(6), 3015–29 (2004).

- 1 ³⁷ W. Humphrey, A. Dalke, and K. Schulten, "VMD: visual molecular dynamics.," J Mol Graph **14**(1), 33–8,
- 2 27–8 (1996).
- 3 ³⁸ S. Kauffmann-Weiss, A. Kauffmann, R. Niemann, J. Freudenberger, L. Schultz, and S. Fähler, "Twinning
- 4 phenomena along and beyond the bain path," Metals (Basel) **3**(4), 319–336 (2013).
- 5 ³⁹ A. Fortini, M. Dijkstra, M. Schmidt, and P.P.F. Wessels, "Wall-fluid and liquid-gas interfaces of model
- 6 colloid-polymer mixtures by simulation and theory," Phys Rev E Stat Nonlin Soft Matter Phys **71**(5), 1–13
- 7 (2005).
- 8 ⁴⁰ F.A. Escobedo, "Tracing coexistence lines in multicomponent fluid mixtures by molecular simulation," J
- 9 Chem Phys **110**(24), 11999–12010 (1999).
- 10 ⁴¹ F.A. Escobedo, "Mapping coexistence lines via free-energy extrapolation: application to order-disorder
- phase transitions of hard-core mixtures.," J Chem Phys **140**(9), 094102 (2014).
- 12 ⁴² I.Q. Matos, and F.A. Escobedo, "Self-Assembling of Nonadditive Mixtures Containing Patchy Particles with
- 13 Tunable Interactions," J Phys Chem B **127**(41), 8982–8992 (2023).
- 14 ⁴³ Y. Wang, Y. Zhou, Q. Yang, R. Basak, Y. Xie, D. Le, A.D. Fuqua, W. Shipley, Z. Yam, A. Frano, G. Arya, and
- 15 A.R. Tao, "Self-assembly of nanocrystal checkerboard patterns via non-specific interactions," Nat Commun
- 16 **15**(1), 3913 (2024).